Single-End Based Fault Location Method for VSC-HVDC Transmission Systems

Elgamasy, Mahmoud M.; Izzularab, Mohamed A.; Zhang, Xiao-ping

DOI:
10.1109/ACCESS.2022.3169777

Document Version
Publisher's PDF, also known as Version of record

Citation for published version (Harvard):
Elgamasy, MM, Izzularab, MA & Zhang, X 2022, 'Single-End Based Fault Location Method for VSC-HVDC Transmission Systems', *IEEE Access*, vol. 10, pp. 43129-43142. https://doi.org/10.1109/ACCESS.2022.3169777

IEEE Access
Multidisciplinary | Rapid Review | Open Access Journal

Received March 23, 2022, accepted April 6, 2022, date of publication April 22, 2022, date of current version April 28, 2022.

Digital Object Identifier 10.1109/ACCESS.2022.3169777

Single-End Based Fault Location Method for VSC-HVDC Transmission Systems

MAHMOUD M. ELGAMASY[1,2], MOHAMED A. IZZULARAB[1], AND XIAO-PING ZHANG[2], (Fellow, IEEE)

[1]Electrical Engineering Department, Faculty of Engineering, Menoufia University, Shebin El-Kom 32511, Egypt
[2]Department of Electronic, Electrical and Systems Engineering, School of Engineering, University of Birmingham, Birmingham B15 2TT, U.K.

Corresponding author: Xiao-Ping Zhang (x.p.zhang@bham.ac.uk)

This work was supported in part by the U.K. Engineering and Physical Sciences Research Council (EPSRC) under Grant EP/N032888/1, and in part by the Egyptian Government Ministry of Higher Education (Cultural Affairs and Missions Sector)/British Council through Newton-Mosharafa Fund.

ABSTRACT A single-end based fault location method is proposed for VSC (Voltage Sourced Converter) HVDC (High Voltage Direct Current) transmission systems. With the proposed method, there is no need for communication system to collect data from different locations and the need for checking data synchronization is avoided. The proposed method is derived from the relationship between the aerial and ground voltage components along the DC transmission system. Bergeron model equations are used for calculating the 1-mode and 0-mode voltages along the transmission system using the measured signals at a single end. The proposed method is generalized for locating both the pole-to-ground and pole-to-pole faults. The profile of the differences between the voltage components is studied with considering the effect of the fault resistance. Artificial neural network (ANN) is trained based on collected samples from different test cases. The proposed single-end based fault location method can successfully locate the fault and determine the fault resistance even with uncertain line parameters. The proposed method is theoretically validated by the help of PSCAD simulation platform. In addition, the effectiveness of the proposed method is verified based on real time measurements obtained from RTDS system.

INDEX TERMS Fault location, fault detection, HVDC, voltage sourced converter (VSC), modular multilevel converter (MMC), energy storage, travelling wave model, pole-to-ground fault, pole-to-pole fault, artificial neural network (ANN), training.

I. INTRODUCTION

VSC (Voltage Sourced Converter) HVDC (High Voltage Direct Current) transmission systems become a highly significant method for various applications in electrical power systems [1]–[4]. In comparison to the CSC (Current Sourced Converter) based HVDC systems, the VSC HVDC systems have the features such as high controllability, no need for reactive power compensation, no commutation failure problems, and more flexible for multi-terminal system operations [5]–[8].

Generally, providing a reliable protection for the VSC-HVDC transmission systems is still an interesting topic for researchers [9]–[16]. Furthermore, locating of faults for the VSC-HVDC transmission system has been considered to be challenging. Successfully locating of DC line faults will reduce the interruption time for maintenance and enhance the system continuous service and operation.

Fault location methodologies are generally categorized into two main types, namely single-end and two-end based methods. The single-end based methods are more distinguished. Depending on the signals captured at a single end of the transmission system avoids the need for verifying data synchronization and there is no need for communication system [17]–[21]. There are many methodologies to locate the DC fault where another categorization of the algorithms can be presented as follows:

A. TRAVELING WAVE METHODS

The traveling wave algorithms are considered among the outstanding techniques in fault location application [22]–[32]. Such methods need to accurately identify the exact instants

The associate editor coordinating the review of this manuscript and approving it for publication was Sarasij Das.

at which the originated traveling waves from the fault point reach the terminals. With the help of the recorded time difference between the waves' arrivals at both ends in addition to the traveling wave speed value, the location of the fault could be figured. However, the accuracy of such methods is significantly affected by the accuracy of identifying the wave arrival instant at terminal, the precision of the traveling wave speed value, and the time synchronization between measured signals at both ends. The corresponding strategy for locating the fault based on single-end measurements has been investigated in [27], [28]. However, such methods need to characterize the initial waveheads in addition to the reflected ones. Furthermore, a discrimination between the reflected waves from the fault point and the others reflected from the remote end is needed to be successfully performed. This brings difficulty in application particularly with the presence of high frequency noise. In addition, these methods are applicable to locate ground faults only as it depends on the existence of the zero-mode components [27], [28].

Other traveling wave methods are introduced with special control arrangements as in [29], [30]. In [29], the modular multilevel converter unit is exploited in injecting a traveling wave pulse to be propagated over the transmission system for locating the ground faults. However, this is exclusive only for the ground faults and MMC-based systems. A similar idea is proposed in [30] where the hybrid DC circuit breaker is controlled such that voltage pulse is injected along the faulty line to determine the fault location. There are other methods based on the same concept however with the requirement for visiting the site and including additional equipment such as specific waveform injector, tracing monitors, and dedicated processing units [31], [32].

B. MACHINE LEARNING METHODS

In terms of artificial intelligence applications, a simple yet low complexity method was proposed in [33], which depends on the similarity of the captured voltage signal at one end of the transmission system to existing patterns. Pearson's correlation coefficient is utilized to detect the similarity of the captured voltage signal at one end of the transmission system to existing patterns. It is successfully applied with CSC-based HVDC transmission systems; however, it could not be applied to VSC-based systems because of the different boundary components and converter types. The concept of employing Pearson's correlation method was used in [34] with a VSC system, and the method relies on checking the similarity of the DCCB branches' currents to existing previously obtained data. After the most correlated patterns are confirmed, kernel-based weighted averaging processing is performed to calculate the accurate fault location. This method needs complex computations with significant computational burdens in data. In addition, it is limited to only the systems employing hybrid DC circuit breakers.

The proposed algorithm in [35] depends on the stacked auto-encoder (SAE) neural network for locating the fault. It is considered as a supplementary to the traveling wave-based fault location methods. It needs to capture the traveling current surges to be used as input to the trained SAE. This necessitates capturing the measured signal at a high sampling rate of 5 MHz. Another study has been presented in [36] without the need to capture traveling wave heads in the time domain. Lower sampling rate of 50 kHz is utilized. However, this method is applicable only with the two-level converter systems with large shunt capacitors at terminals. The shunt capacitors help to simplify the expression of natural frequency to be related the distance of the fault. More investigation is still required with different systems such as the MMC systems where the capacitors are not lumped at terminals with such cases.

C. TIME DOMAIN CALCULATION METHODS

With regard to the time-domain based calculations, the Bergeron model representation has been successfully employed in proposing fault location method with utilizing measurements at both ends [17], [18]. The profile of 1 -mode voltage is calculated over the length of the transmission system by the help of Bergeron model equations in terms of the local measured signals. Two 1 -mode voltage profiles are obtained as the calculations are performed with respect to each end. Then, the fault point could be identified by the point at which the calculated 1 -mode voltages are equal. In [37], the fault location could be identified based on using the data measured at two ends of the transmission system. It is based on creating an estimated simple R-L model for the transmission system to provide a formula for the fault location. It is a high accurate method but needs long time window for the post fault data in order to get a stable result without fluctuations in the determined value for the fault location.

Based on Bergeron model equations, the proposed method in this paper is developed. The proposed method is a single-end based method, and hence there is no need for communication system and the problem of unsynchronized samples is avoided. The relation between the 1-mode and 0-mode components of the voltage along the transmission system with considering the fault resistance value helps identify the fault location. The introduced method is based on training ANN (artificial neural network) for determining the fault location. The proposed method is successful in locating both the pole-to-ground and pole-pole faults in monopole and bi-pole systems and the proposed method is a generalized method as single processing core is adopted for locating both fault types.

The paper is organized as follows; in section II, the proposed fault location method is explained. Section III shows the obtained results considering the performance of the trained ANN. In section IV, the performance of the proposed method is studied with utilizing uncertain parameters of the transmission system. The proposed method is extra validated considering different monopole MMC based system running in real time by the help of RTDS in section V. The impact of AC side grid on the proposed method is tested in section VI. Finally, the conclusion is presented in section VII.

II. FAULT LOCATION METHOD

A. PROPOSED METHOD

The fault location could be determined based on the relation between the 1-mode and 0-mode voltages along the transmission line.

1) POLE-TO-GROUND FAULTS

With considering a severe pole-to-ground fault condition as shown in Fig. 1 (a), the following conditions are met at the fault location:

$$V_p = 0, \quad I_p = I_f, \; I_n = 0 \tag{1}$$

where V_p is the voltage of the positive pole at the fault location, I_p and I_n are the positive and negative poles currents at the fault point. The 1-mode and 0-mode voltages and currents at the fault location could be calculated from the following equations:

$$\begin{bmatrix} V_1 \\ V_0 \end{bmatrix} = \frac{1}{\sqrt{2}} \begin{bmatrix} 1 & -1 \\ 1 & 1 \end{bmatrix} \begin{bmatrix} V_p \\ V_n \end{bmatrix}, \quad \begin{bmatrix} I_1 \\ I_0 \end{bmatrix} = \frac{1}{\sqrt{2}} \begin{bmatrix} 1 & -1 \\ 1 & 1 \end{bmatrix} \begin{bmatrix} I_p \\ I_n \end{bmatrix} \tag{2}$$

$$V_1 = -V_0 = \frac{-1}{\sqrt{2}} V_n, \quad I_1 = I_0 = \frac{1}{\sqrt{2}} I_f \tag{3}$$

Using (3), the relation between the 1-mode and 0-mode equivalent circuits could be derived as shown in Fig. 1 (b).

2) POLE-TO-POLE OR DOUBLE POLE-TO-GROUND FAULTS

The pole-to-pole fault case is similar to double pole-to-ground condition. In both cases, there is no current to the ground because the two poles are balanced as depicted in Fig. 1 (c). In both cases, the following conditions are met at the fault location:

$$V_p = V_n = 0, \quad I_p = I_f = -I_n \tag{4}$$

$$V_1 = V_0 = 0, \quad I_0 = 0, \; I_1 = \sqrt{2}\, I_f \tag{5}$$

With this balanced condition between the poles, the 1-mode and the 0-mode circuits are not interconnected at the fault point as indicated in Fig. 1 (d). The 0-mode circuit is not active and there is no flowing 0-mode current and thus the 0-mode voltage is zero as well. The system condition is represented only by the 1-mode circuit and the 1-mode voltage level at the fault point is zero.

B. PROPOSED FORMULA

The key generalized feature for determining the fault location for both the ground and pole faults is that the absolute values of the 1-mode and 0-mode voltage components are equal at the fault point. The voltage components can be calculated along the whole length of the transmission system in terms of the locally measured signals at one end of the transmission system as indicated in Fig. 2. The Bergeron model equations used for calculating the 1-mode and 0-mode voltages along the transmission system are presented in appendix A. The voltage components are obtained as follows:

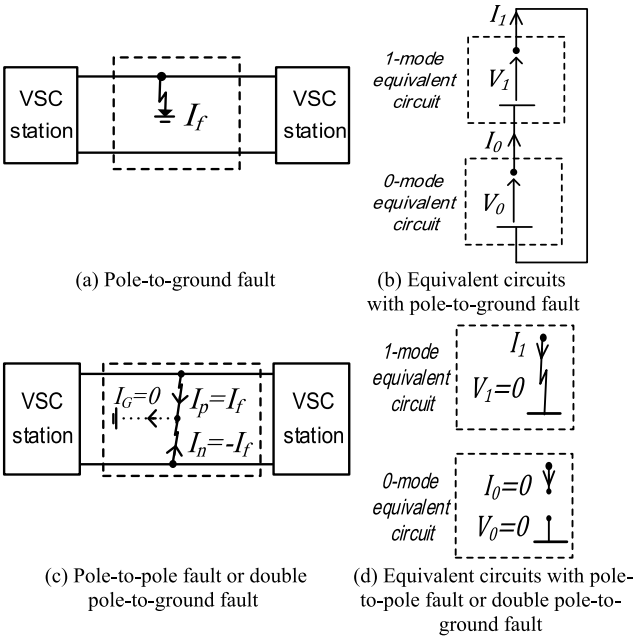

FIGURE 1. The aerial mode and ground mode circuits during fault condition.

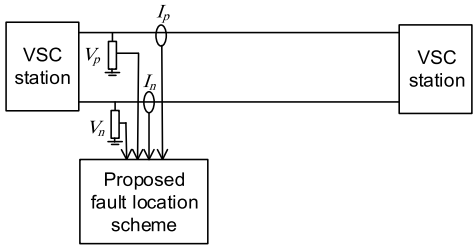

FIGURE 2. Signals measured at one end of the transmission system for implementing the proposed fault location method.

$$\widetilde{V}_1(x) = \frac{\sum_{t_1}^{t_2} |V_1(\mathbf{x})|}{(t_2 - t_1)/\Delta t}, \quad \widetilde{V}_0(x) = \frac{\sum_{t_1}^{t_2} |V_0(\mathbf{x})|}{(t_2 - t_1)/\Delta t} \tag{6}$$

$$\Delta V\,(x) = \left|\widetilde{V}_1\,(x) - \widetilde{V}_0(x)\right| \tag{7}$$

where $\widetilde{\boldsymbol{V}}_{\mathbf{1}}(\boldsymbol{x})$, $\widetilde{V}_0(\boldsymbol{x})$re the normalized values for the 1-mode and 0-mode calculated voltages at specific location x during the post-fault duration from $\boldsymbol{t_1}$ to $\boldsymbol{t_2}$. $\boldsymbol{t_1}$ is the instant at which the 1-mode voltage at the line terminal gets below 0.9 pu. Δt is the sampling time step. $\boldsymbol{V_1}$ (x) and $\boldsymbol{V_0}$ (x) are calculated with the help of Bergeron model equations in terms of the single-end measurements. ΔV is the difference between aerial mode and ground mode voltages. Because the 1-mode and 0-mode voltages are equal at the fault point, ΔV would be zero. Then the fault location could be determined as follows:

$$\Delta V\,(fault\_loc) = \min\{\Delta V\,(x) : x \in (0, total\_length)\} \tag{8}$$

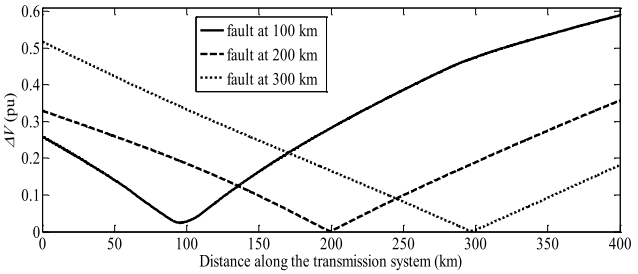

(a) Voltage difference profile under sever pole-to-ground fault cases

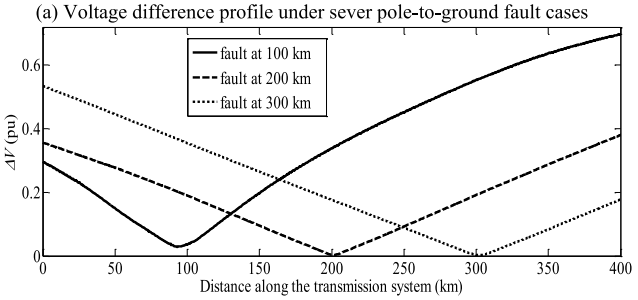

(b) Voltage difference profile under severe pole-to-pole fault cases

FIGURE 3. The difference between the aerial mode and ground mode voltages calculated based on single-end measurements.

C. PROFILE OF THE DIFFERENCE BETWEEN 1-MODE AND 0-MODE VOLTAGE COMPONENTS

For the investigation of the profile of the difference between the 1-mode and 0-mode voltages, a bipolar HVDC system of 400 MW, ±400 kV, 400 km is simulated using PSCAD. The details about the configuration of the transmission system will be presented in the next section. A frequency dependent model for the employed transmission system is utilized to obtain accurate simulated results. The converter units are two-level-based types and represented by their detailed models. The sampling time step is 20 μs. Different severe pole-to-ground and pole-to-pole fault cases are tested at 100 km, 200 km, and 300 km, respectively. The samples are collected from the test cases on PSCAD, then they are processed offline using Matlab. The 1-mode and 0-mode voltage distributions are calculated along the transmission system for each case. Then, the voltage difference versus the distance along the transmission system according to (7) can be determined. Figs. 3 (a) and 3 (b) show the obtained results for the voltage difference profile for pole-to-ground and pole-to-pole faults, respectively. As shown in the figures, the voltage difference profile reaches a minimum value at the fault location. These cases are for severe faults where the fault resistance is almost zero. While the following section will discuss the aspects of fault resistances.

D. CONSIDERATION OF THE FAULT RESISTANCE

1) POLE-TO-GROUND FAULTS

With the pole-to-ground fault condition with fault resistance, the following conditions are met at the fault location:

$$V_p = I_f R_f, \quad I_p = I_f, \; I_n = 0 \tag{9}$$

After calculating the 1-mode and 0-mode signals, the following relations are obtained:

$$I_1 = I_0 = \frac{1}{\sqrt{2}} I_f \tag{10}$$

$$V_1 = \frac{1}{\sqrt{2}} V_p - \frac{1}{\sqrt{2}} V_n, \quad V_0 = \frac{1}{\sqrt{2}} V_p + \frac{1}{\sqrt{2}} V_n \tag{11}$$

From (10) and (11), the relation between the 1-mode and 0-mode voltages is as follows:

$$V_1 + V_0 = \sqrt{2}\, V_p = \sqrt{2}\, I_f R_f \tag{12}$$

$$V_1 + V_0 = 2 I_1 R_f \tag{13}$$

The equivalent circuits' connection is as shown in Fig. 4 (a). The difference between the 1-mode and 0-mode voltages would not be zero at the fault location. In other expression, (7) is updated as follows:

$$\Delta V\left(x, R_f\right) = \left|\widetilde{V}_1\left(x, R_f\right) - \widetilde{V}_0\left(x, R_f\right)\right| = 2 I_1 R_f \tag{14}$$

As seen in (14), the voltage difference is affected by the fault resistance value. For investigating this aspect, pole-to-ground fault cases are tested at 200 km distance with changing the fault resistance value. Fig. 4 (b) shows the voltage difference profile calculated with changing the fault resistance value. As depicted, the obtained profile is shifted and it depends on the resistance value.

2) POLE-TO-POLE FAULTS OR DOUBLE POLE-TO-GROUND FAULTS

With having a pole-to-pole or double pole-to-ground fault condition via a fault resistance, the signals at the fault location are defined as:

$$V_p - V_n = I_f R_f, \quad V_p = I_f \frac{R_f}{2}, \; V_n = -I_f \frac{R_f}{2} \tag{15}$$

$$I_p = I_f = -I_n \tag{16}$$

$$V_1 = \frac{1}{\sqrt{2}}\left(V_p - V_n\right) = \frac{1}{\sqrt{2}} I_f R_f \tag{17}$$

$$I_0 = 0, \quad I_1 = \frac{1}{\sqrt{2}}\left(I_p - I_n\right) = \frac{2}{\sqrt{2}} I_f \tag{18}$$

$$V_0 = 0, \quad V_1 = I_1 \frac{R_f}{2} \tag{19}$$

It is worthy to note that the fault resistance in case of double pole-to-ground fault is assumed to be balanced. The unbalanced double pole-to-ground fault is to be considered in future study. The fault resistance value affects the 1-mode voltage and consequently the voltage difference profile long the transmission system. Fig. 4 (c) indicates the fault resistance in the equivalent circuit and Fig. 4 (d) shows the testing results of the pole-to-pole fault cases at 200 km distance with varying the fault resistance.

E. ANN FOR LOCATING THE FAULT

Based on the abovementioned analysis, each fault location has a set of profiles of the difference between the 1-mode and 0-mode voltages. Various profiles are obtained because of

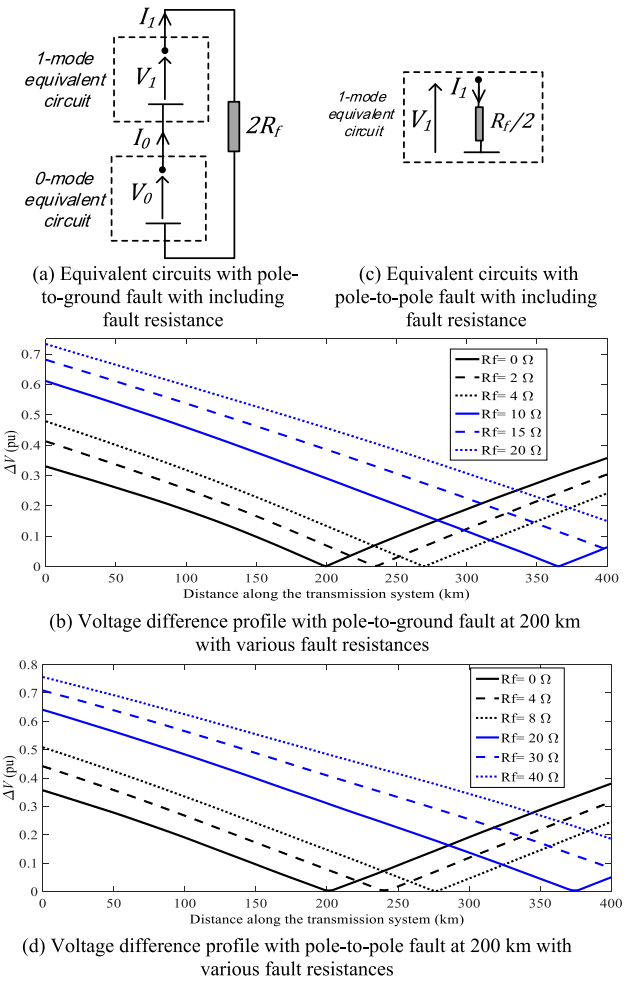

(a) Equivalent circuits with pole-to-ground fault with including fault resistance

(c) Equivalent circuits with pole-to-pole fault with including fault resistance

(b) Voltage difference profile with pole-to-ground fault at 200 km with various fault resistances

(d) Voltage difference profile with pole-to-pole fault at 200 km with various fault resistances

FIGURE 4. **The equivalent circuits and voltage difference with considering the fault resistance influence.**

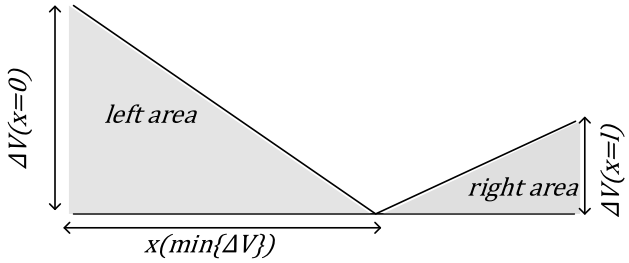

(a) The features of the voltage difference profile as inputs for the neural network.

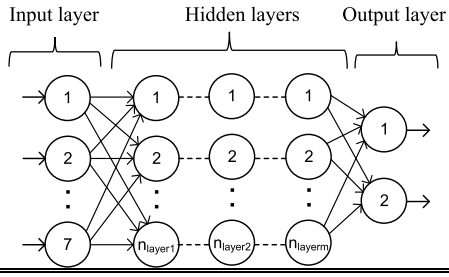

	NN Inputs	NN Outputs
Features extracted from the profile of ΔV as in Fig. 5 (a)	*1-* $\Delta V\ (x=0)$ *2-* $\Delta V\ (x=l)$ *3-* $x(\min\{\Delta V\})$ *4-* *Left area* *5-* *Right area*	*1-* Fault location *2-* Fault resistance
Additional inputs	*6-* $(V_0 >$ *threshold): True / false* *7-* *Max* (di_1/dt)	

(b) Detailed inputs and outputs for the neural network.

FIGURE 5. **Neural network design.**

the effect of the fault resistance value. The proposed method depends on training neural network for locating the fault and determining the fault resistance value as well. The proposed method is designed based on adopting single neural network for locating both ground and pole-to-pole fault types. The features extracted from the voltage difference profile represent the main inputs to the neural network. These features represent 5 inputs as indicated in Fig. 5 (a). In addition, there are extra 2 inputs to the neural network which support better identifying the fault location. Fig. 5 (b) shows a typical configuration of the neural network and all the inputs and outputs are indicated in the table in Fig. 5 (b).

The first one of the additional inputs is the condition of the 0-mode voltage. This input is true/false type which indicates the existence of 0-mode voltage or not. This helps to identify the fault type. The pole-to-ground faults result in the existence of high value of the 0-mode voltage because of the unbalance between the poles. On the other hand, there is no 0-mode voltage with pole-to-pole or double pole-to-ground faults. Thus, the ground and pole faults could be extinguished by the help of this input. It is worthy to note that the threshold value for discriminating the existence of the 0-mode voltage is selected to be 0.2 pu [11]. The second one of the additional inputs is the maximum value of the rate of change of the 1-mode current measured at the terminal. The 1-mode current exists in all fault types. This helps discriminate the cases which are quite similar in the voltage difference profile. As an example, the voltage difference profiles of two different fault cases at 150 km with $R_f = 10\ \Omega$ and 315 km with $R_f = 0\ \Omega$, respectively are shown in Fig. 6 (a) where both profiles are quite similar. However, the maximum value of the rate of change of the 1-mode current measured at the terminal is different and discriminative as presented in Fig. 6 (b). Thus, the proposed neural network has 7 inputs, 2 outputs, and the number of hidden layers is indicated in the following section III.A

III. VALIDATION OF RESULTS

A. ANN TRAINING

Samples are needed to be collected for training the neural network. With referring to the simulated system in II.C, variant test cases for pole-to-ground and pole-to-pole faults are simulated. Different fault locations are tested starting at 0 km up to 400 km with a step of 10 km between cases; and for each fault location, different fault resistances are considered, such as 0, 2, 3, 4, 5, 6, 7, 8, 9, 10, 15, 20, 25, 30, and 35 Ω for pole-to-ground faults and 0, 4, 6, 8, 10, 12, 14, 16, 18, 20, 30, 40, 50, 60, and 70 Ω for pole-to-pole faults.

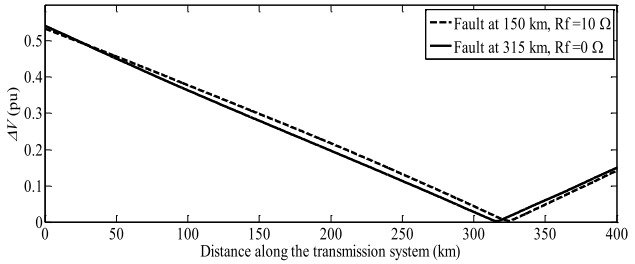

(a) The voltage difference profile for two different fault cases at different locations

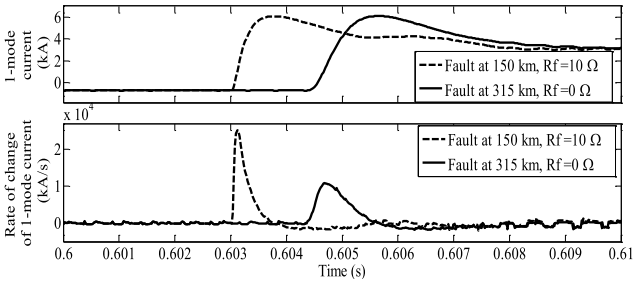

(b) The 1-mode currents and its rate of change for two different fault cases at different locations

FIGURE 6. Rate of change of the 1-mode current considering two different fault locations having the same voltage difference profile.

With Matlab tool, a single neural network is trained using the collected data sets. The inputs are normalized before the training. The single neural network consists of 4 hidden layers with 15 neurons for each layer. The data set is divided whereas 80% of the data set is for training, 10% for testing, and 10% for validation. The performance of the trained NN is as shown in Fig. 7 (a) where best validation performance is 8.5878e-05 at epoch 288. Regression analysis is performed and a high correlation is obtained between the outputs and targets for locating the fault. The regression coefficient is 0.99985 for the data set employed for training, 0.99971 for the tested samples, and 0.9997 for the validated data as shown in Figs. 7 (b), 7 (c), and 7(d), respectively. Figs. 7 (e) and 7 (f) show the error between the outputs and targets of the trained network for locating the fault. The error is measured as a percentage of the total transmission system length of 400 km. At each fault location, there are many samples for the error because of the various corresponding test cases. The figure shows the error samples put in ascending order at each location. The central red mark in each box indicates the median values of the errors, and the bottom and top edges of the box indicate the 25th and 75th percentiles, respectively. The whiskers are extended to the most extreme data points, and the outliers are plotted individually using the '+' symbol. As shown, the error is lower than 1 % for most of the samples.

For further validating the performance of the neural network, it is tested with other samples which are not included in the training process. Different locations and new values for the fault resistance are adopted. Table 1 shows the error values for the adopted test cases.

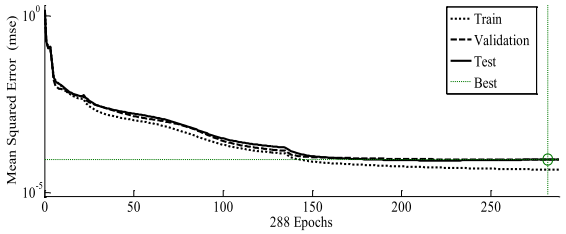

(a) The performance of the trained neural network

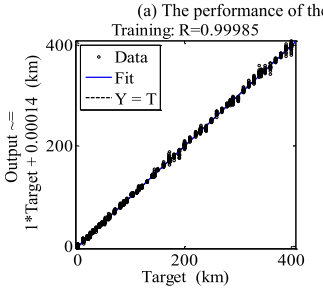

(b) Regression analysis for the trained data set

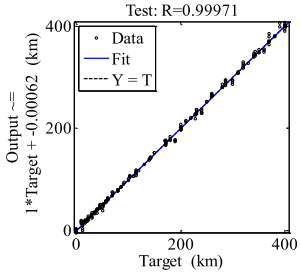

(c) Regression analysis for the tested data set

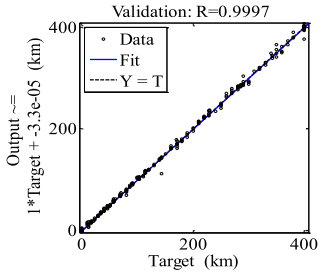

(d) Regression analysis for the validated samples

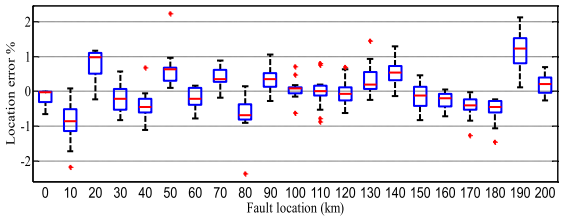

(e) Error between target and output of the trained network for the distance from 0 km up to 200km

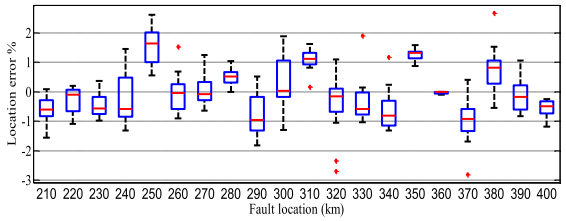

(f) Error between target and output of the trained network from 210 km up to 400 km

FIGURE 7. Performance and regression analysis of the trained neural network for locating the faults.

B. COMPARISONS BETWEEN PROPOSED METHOD AND OTHER EXISTING RELATED METHODS

Table 2 presents the fault location error values for both the proposed method and other existing related methods. The mean and maximum values of the proposed method errors are calculated based on the results in Table 1 where the neural network has been tested with new cases not included

TABLE 1. Testing the trained NN with new test cases.

Fault Type	Fault location (km)	Fault Resistance (Ω)	Neural Network outputs		Error in location %
			Location (km)	Fault resistance	
PG	5	0.7	5.79	3.07	0.1985
PP	5	0.7	6.89	0.39	0.4742
PP	5	9.5	9.21	9.29	1.0546
PP	8	2	3.66	2.5	1.0842
PG	12	27	6.58	25.39	1.3528
PP	22	11	19.52	11.14	0.6188
PG	44	2	40.43	1.23	0.8936
PP	64	34	57.79	34.43	1.5501
PG	131	6.5	130.39	6.63	0.1504
PP	150	25	150.01	23.32	0.0007
PG	175	22	174.66	22.64	0.0854
PP	194	75	197.05	67.31	0.7642
PG	243	5.5	243.99	6.20	0.2488
PP	274	0	274.04	2.02	0.0123
PP	298	45	288.40	46.06	2.3991
PP	304	47	300.22	47.72	0.9442
PG	312	0	312.12	1.17	0.0300
PP	327	7.5	325.74	7.17	0.3150
PP	355	33	349.64	36.05	1.3408
PG	372	4.4	372.43	5.75	0.1084
PP	375	15	373.04	16.43	0.4900
PP	392	3	392.06	4.12	0.0149

TABLE 2. Performance evaluation compared to existing related methods.

		Fault location Error		
		Mean value	Maximum value	
1	Proposed method	0.64 %	2.39 %	
2	SAE method	0.71 %	1.23 %	as reported in [35]
3	ANN with wavelet coefficients as input	1.59 %	2.36 %	
4	Single-end traveling wave method	2.03 %	5.31 %	

in the training. The second algorithm in the table is based on training SAE neural network and uses the captured current surges as input. The third algorithm depends on extracting the wavelet coefficients of the measured current and use it as input to a trained neural network. In addition, the performance of single-end traveling wave method is included. As shown, the proposed method is distinguished by having the lowest value of the mean error. From the maximum error values, it is indicated that the SAE method is the best algorithm. However, very high sampling frequency is mandatory with this method where 5 MHz is utilized to capture the current surges while the proposed method is validated with 50 kHz. Furthermore, the proposed method is implemented with lower sampling rate at 20 kHz and 10 kHz as indicated in sections V.A and VI respectively. The third and fourth methods in the table are limited by higher errors and the need for high sampling rate as well.

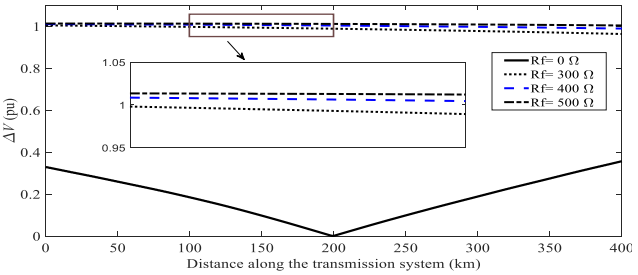

(a) The voltage difference profile with much higher fault resistances.

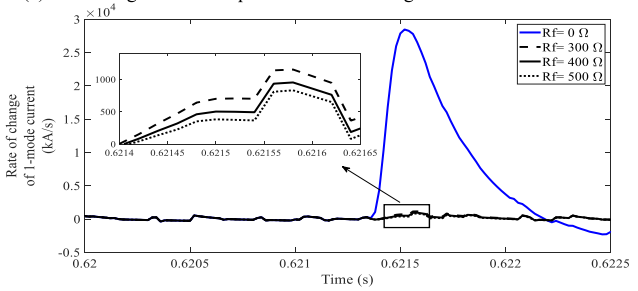

(b) The rate of change of the 1-mode current with much higher fault resistances.

FIGURE 8. Effect of much higher fault resistances.

C. MUCH HIGHER FAULT RESISTANCE

The proposed method is tested under much higher fault resistances. Pole-to-ground fault cases at 200 km with having fault resistance of 300, 400, and 500 Ω are simulated. The effect of low resistance values is previously shown in Fig. 4 (b). In this section, Fig. 8 (a) indicates the profile of ΔV with having high fault resistances. The profile of ΔV at 0 Ω fault resistance is included for better indicating the effect due to the much high resistances. In addition, Fig. 8 (b) shows the rate of change of 1-mode current considering these test cases. As shown, both of the profile of ΔV and the rate of change of the 1-mode current become not discriminative enough with much higher fault resistances.

IV. UNCERTAINTIES IN LINE PARAMETERS

A. INFLUENCE ON VOLTAGE DIFFERENCE PROFILE

The performance of the proposed method is tested if there is uncertainty with the employed parameters. Table 3 shows the previously employed parameters in training and testing in addition to the changed values. The configuration of the corresponding transmission system is shown in Fig. 10.

In order to investigate the effect on the voltage difference profile due to utilizing uncertain parameters, Fig. 9 shows the profile of the voltage difference with a severe pole-to-ground fault condition at 150 km with changing the employed parameters in calculating the voltage difference profile. As depicted, the profile is apparently affected if the parameters are not accurate. It can be found that the performance of the neural network is not badly affected if this deviation in voltage difference profile is considered in the training, and this will be discussed in the following subsection.

TABLE 3. Employed parameters for the training and testing.

r1	0.1170 [Ω/m]	r0	0.1193 [Ω/m]
Zc1	19.9028 [Ω]	Zc0	17.5548 [Ω]
v1	9.4892e+04 [km/s]	v 0	1.0758e+05 [km/s]
CHANGED VALUES FOR THE PARAMETERS FOR CHECKING THE UNCERTAINTY			
r1	0.1236 [Ω/m]	r0	0.1231 [Ω/m]
Zc1	17.2828 [Ω]	Zc0	17.0420 [Ω]
v1	1.0928e+05 [km/s]	v 0	1.1082e+05 [km/s]
CHANGING PERCENTAGE			
r1	+5.64 %	r0	+3.18 %
Zc1	-13.16 %	Zc0	-2.92 %
v1	+15.16 %	v 0	+3.01 %

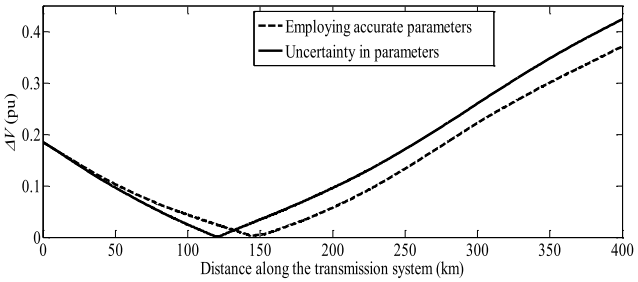

FIGURE 9. Influence of inaccurate parameters on the voltage difference profile with severe ground fault at 150 km.

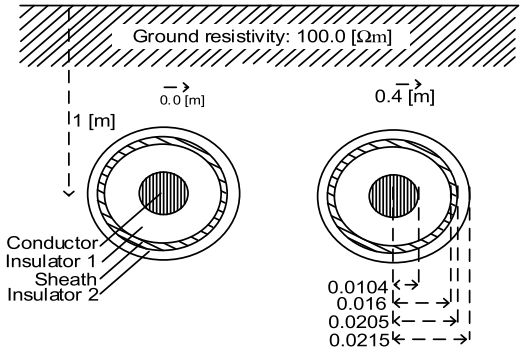

FIGURE 10. Configuration of the employed underground cable [10], [11].

B. ANN PERFORMANCE WITH UNCERTAIN PARAMETERS

Firstly, it should be pointed out that the parameters are included for calculating the voltage difference profile in two steps:

a) Training: The parameters are utilized for creating the voltage difference profiles for training the neural network. This is performed with the help of collected data of predefined cases.
b) Functioning: After establishing the network, the parameters are needed in calculating the voltage difference profile for locating the fault. This is performed for new cases not included in training.

It is found that the proposed method is not affected by the uncertain parameters if the deviated voltage difference profile is considered in the training of the neural network and the same parameters are included in both training and functioning of the neural network.

The uncertain parameters indicated in table 3 is utilized for retraining and testing a new neural network. By using the collected samples in section II, the voltage difference profiles are regenerated by utilizing the changed parameters according to Table 3; and neural network is retrained. Firstly, the performance of the retrained NN is studied. It indicates in Fig. 11 (a) where the best validation performance is 6.2919e-05 at epoch 443. Furthermore, regression analysis is performed. It is found that a high correlation is obtained between the outputs and targets for locating the fault. The regression coefficient is 0.99948 for the data set employed for the training, 0.99908 for the tested samples, and 0.99905 for the validated data as shown in Figs. 11 (b), 11 (c), and 11 (d), respectively. Figs. 11 (e) and 11 (f) show the error between the outputs and targets of the retrained network for locating the fault with using uncertain parameters. As shown, the error is lower than 1 % for most of the samples despite the uncertainty in parameters.

Furthermore, the performance of the retrained neural network is tested with new cases which are not included in the training process. It is worthy to note that the same uncertain values for the parameters are utilized. The new cases which are previously tested according to Table 1 are adopted again in Table 4.

Table 4 shows the results obtained for the tested fault cases. As shown, the error is lower than 1% for most of the samples although of employing uncertain parameters. This is a great advantage of the proposed method where it shows stable performance even with uncertain parameters. This is because the deviated voltage difference profile is considered in the training and the same parameters are included for both the training and functioning of the neural network.

V. VALIDATION WITH MONOPOLE MMC SYSTEM ON RTDS

The above validation analysis was simulated for a bipolar 400 km HVDC system with underground cable configuration on PSCAD software. For more validating the proposed fault location method, another monopole MMC-based system is implemented on RTDS.

It is worthy to note that the bipolar and monopolar systems are different in configuration. A brief description about the difference between bipolar and monopolar systems is presented in appendix B. Validating the proposed method with monopolar system extra supports the efficacy of the proposed method.

Fig. 12 (a) shows a block diagram for the test system. It is a two-terminal monopole 100 MW, 60 kV MMC based HVDC system. Overhead transmission line of 100 km is employed according to the configuration depicted in Fig. 12 (b) and its frequency dependent model is implemented for more accurate representation. In order to validate the proposed fault location method, suitable data set is firstly established

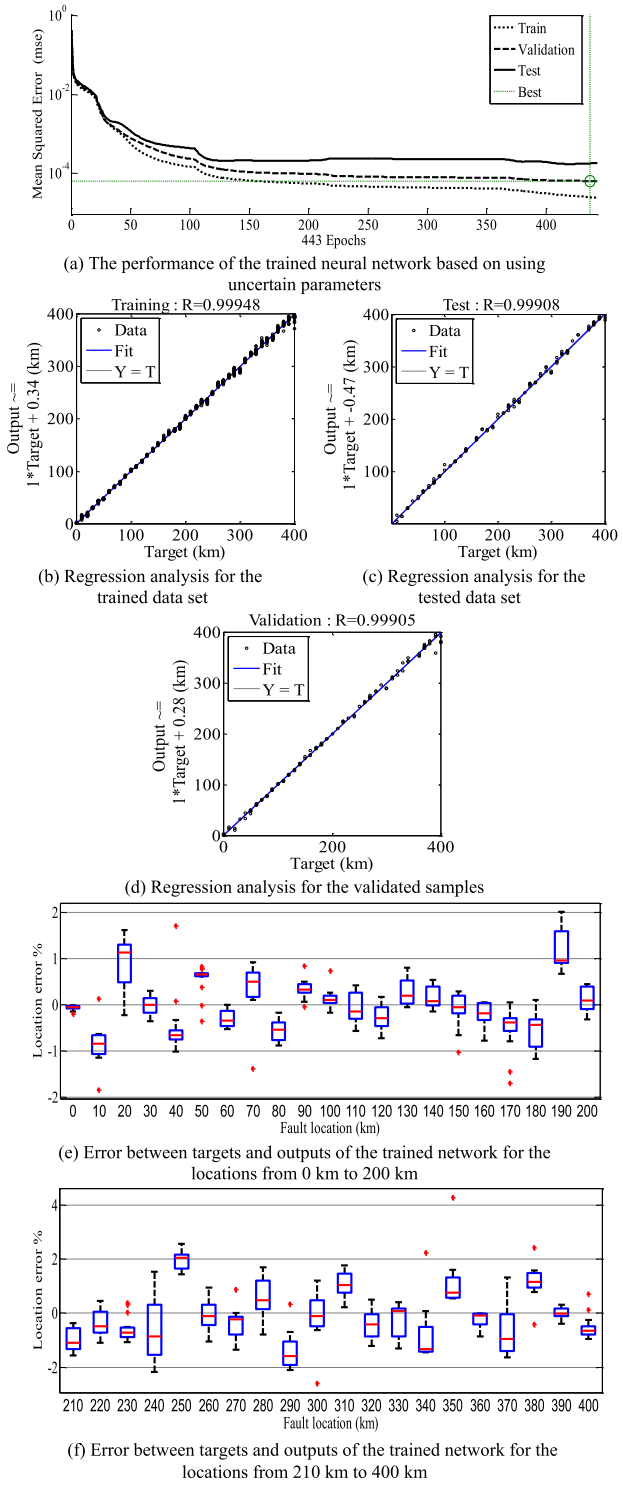

(a) The performance of the trained neural network based on using uncertain parameters

(b) Regression analysis for the trained data set

(c) Regression analysis for the tested data set

(d) Regression analysis for the validated samples

(e) Error between targets and outputs of the trained network for the locations from 0 km to 200 km

(f) Error between targets and outputs of the trained network for the locations from 210 km to 400 km

FIGURE 11. Performance and regression analysis of the retrained neural network with utilizing uncertain parameters.

based on testing different fault cases with the adopted system on RTDS. Then, the collected data set are utilized for validating the proposed fault location method offline by Matlab.

TABLE 4. Testing the retrained NN after changing the parameters.

Fault Type	Fault location (km)	Fault Resistance (Ω)	Neural Network outputs		Error in location %
			Location (km)	Fault resistance	
PP	5	0.7	4.18	3.38	0.20
PP	5	9.5	6.32	9.91	0.33
PG	5	0.7	1.28	1.25	0.92
PP	8	2	3.19	4.74	1.20
PG	12	27	8.08	27.12	0.97
PP	22	11	21.07	10.14	0.23
PG	44	2	37.14	1.93	1.71
PP	64	34	62.12	34.32	0.46
PG	131	6.5	129.31	6.38	0.42
PP	150	25	150.63	25.94	0.15
PG	175	22	179.18	21.28	1.04
PP	194	75	195.98	67.04	0.49
PG	243	5.5	239.01	5.38	0.99
PP	274	0	274.34	2.79	0.08
PP	298	45	288.20	45.92	2.44
PP	304	47	299.22	47.98	1.19
PG	312	0	314.13	1.90	0.53
PP	327	7.5	325.11	8.29	0.47
PP	355	33	348.16	35.90	1.70
PG	372	4.4	377.22	4.34	1.30
PP	375	15	372.64	16.75	0.58
PP	392	3	393.93	4.19	0.48

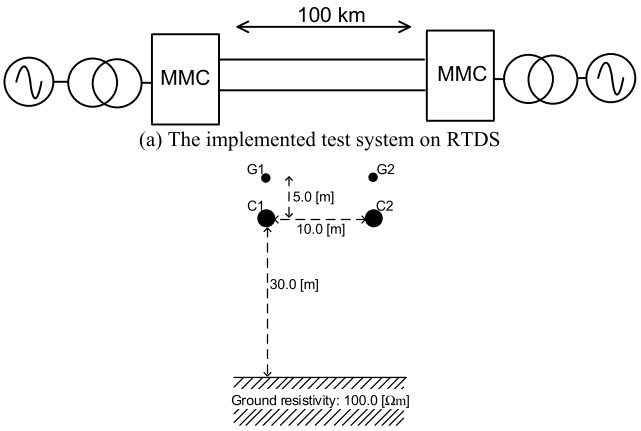

(a) The implemented test system on RTDS

(b) Configuration of overhead transmission system

FIGURE 12. Implemented test system on RTDS.

A. HANDLING LIMITATION OF LARGE STEP IN CALCULATIONS DUE TO LOW SAMPLING FREQUECY

The proposed fault location method needs to calculate the profile of both 1-mode and 0-mode voltages along the transmission system. Then, the difference between both the voltage components helps identify the location of the fault. With the adopted test system on RTDS, a restriction point is determined. The calculated profiles along the transmission system length are found to be more stable and accurate with utilizing large distance step. This is because the time step with RTDS for collecting data is 50 μs and the transmission system is overhead line. With the overhead line configuration,

the traveling wave is faster in propagation than that of the case with underground cable [10], [11]. 50 μs time step size approximately equals the travel time duration along 15 km of the adopted overhead line. This means that the voltage profile can be more accurately calculated every 15 km in distance which is not a good resolution in determining the exact fault location point.

Fig. 13 (a) shows the profiles of the 1-mode and 0-mode components with 15 km large time step in calculations for a fault condition at 50 km. It is an accurate result where both the profiles have the intersection at 50 km which is the exact location of the fault. However, if the difference between both the profiles is calculated with these large step samples, the minimum value of the difference would refer to an inaccurate location. It is hence recommended to have few meters only as a step in calculating the voltages profiles along the transmission system so as to identify the fault location accurately. For handling the abovementioned limitation, the profile of each voltage component is interpolated before calculating the difference.

With interpolating each voltage component profile, more discrete points can be obtained with a step size of a few meters only and the minimum value of the difference would lead to the accurate fault location. Fig. 13 (b) is a representation of the same profiles in Fig. 13 (a) with being interpolated. Fig. 13 (c) indicates the importance of the interpolation where the voltage difference profile is shown with and without the interpolation. As depicted, the minimum value of the difference profile refers to the exact fault location at 50 km with interpolation.

This handling step supports the wide applicability of the proposed fault location method. The fault location could be successfully identified regardless of the configuration of the transmission system for both the overhead and underground systems. In addition, low levels of sampling frequency are acceptable and this is validated by implementing the proposed method with using 10 kHz sampling rate as indicated in the section VI.

B. TEST RESULTS

The concept of the proposed fault detection method is tested on RTDS. Three severe pole-to-ground and pole-to-pole fault cases are implemented at 20 km, 50km, and 80 km, respectively. The measured samples of the voltages and currents at one end of the transmission system are firstly collected. Then, these data are processed offline using Matlab. Fig. 14 shows the profile of the difference between the 1-mode and 0-mode voltages for both ground and pole faults. As shown in the figure, it is highly discriminative profiles to successfully locate the fault even the system is monopole MMC based HVDC.

It is concluded that the proposed method works well with both bipolar and monopolar systems. The proposed method is mainly depending on the voltage profile along the transmission system which is highly affected in both systems. This is a good advantage of the proposed method as it is a general method and the included results in the manuscript provide

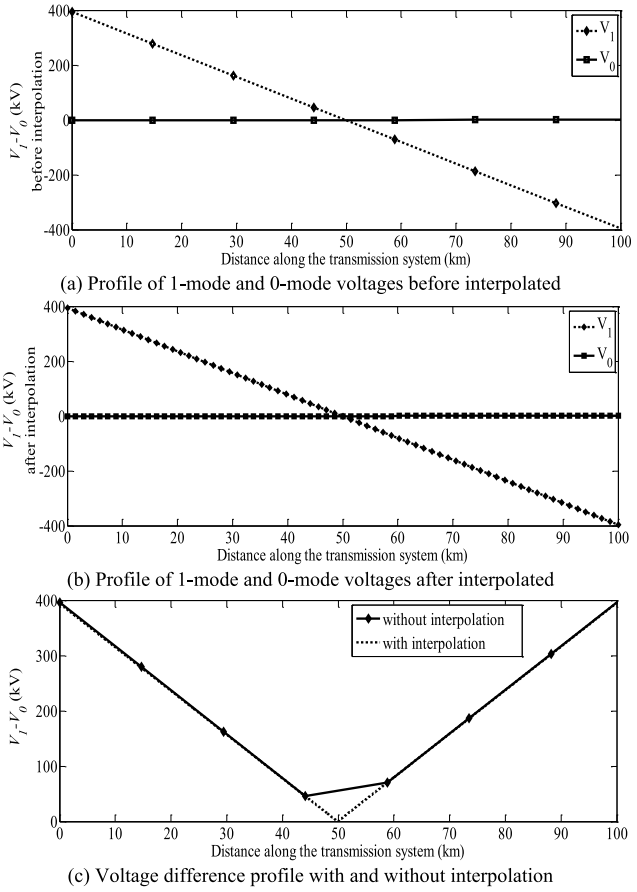

FIGURE 13. Profile of difference between 1-mode and 0-mode voltages with the fault at 50 km.

evidence about the high efficacy of the proposed method for both bipolar and monopolar systems.

C. NEURAL NETWORK TRAINING

Variant test cases for pole-to-ground and pole-to-pole faults are executed on RTDS. Different fault locations are included starting at 0 km up to 100 km with a step of 10 km between cases. For each fault location, variant fault resistances are included starting from 0 Ω to 10 Ω with having a step of 1 Ω and from 12 Ω to 20 Ω with a step of 2 Ω.

With Matlab, a single neural network is trained using the collected data sets. 4 hidden layers are included with 15 neurons for each layer. The data set is divided whereas 80% of the data set is for training, 10% for testing, and 10% for validation. Regression analysis is performed and a high correlation is obtained between the outputs and targets for locating the fault. The regression coefficient is 0.99877 for the data set employed for training, 0.9986 for the tested samples, and 0.99942 for the validated data as shown in Figs 15 (a), 15 (b), and 15 (c), respectively.

Fig. 15 (d) shows the error between the outputs and targets of the trained network for locating the fault. As shown, the error is lower than 1 % for most of the samples. The error

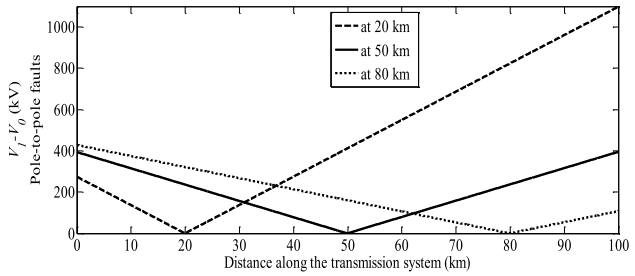

(a) Profile of difference between 1-mode and 0-mode voltages under pole-to-pole faults

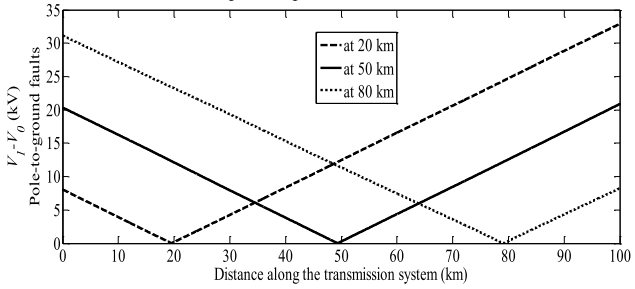

(b) Profile of difference between 1-mode and 0-mode voltages under pole-to-ground faults

FIGURE 14. Profile of difference between 1-mode and 0-mode voltages based on RTDS results.

TABLE 5. Testing the trained NN with new test cases based on RTDS results.

Fault Type	Fault location (km)	Fault Resistance (Ω)	Neural Network Output	
			Location (km)	Error %
PG	6	2	7.7526	1.752
PG	15	11	14.0644	0.935
PG	33	33	34.6886	1.688
PG	66	15	65.9553	0.044
PG	75	7	76.7180	1.718
PG	96	10	97.3664	1.366
PP	3	13	0.0726	2.927
PP	21	5	21.0115	0.011
PP	47	22	45.6625	1.337
PP	65	1	64.3638	0.636
PP	77	8	77.5400	0.540
PP	85	18	84.5101	0.489
PP	91	0	91.2300	0.229

is measured as a percentage of the total transmission system length which is 100 km.

For further validating the performance of the neural network, it is tested with other samples which are not included in the training. Different locations and new values for the fault resistance are adopted. Table 5 shows the results obtained for the tested fault cases. As shown in the table, the error is lower than 1% for most of the samples.

VI. VALIDATION WITH CONVERTER INTERFACED GENERATION AT AC SIDE

The VSC-HVDC systems are widely employed in integrating renewable wind energy resources with the grid. The most common generation types used in wind farms are doubly fed induction generators (DFIG) and permanent magnet

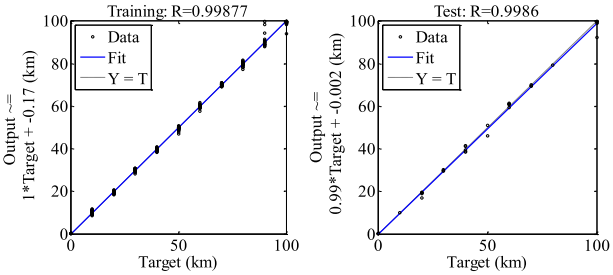

(a) Regression analysis for the trained data set

(b) Regression analysis for the tested data set

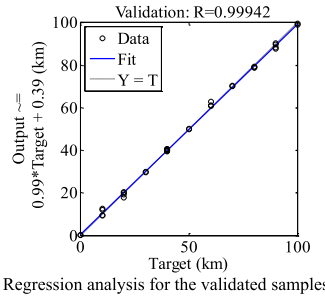

(c) Regression analysis for the validated samples

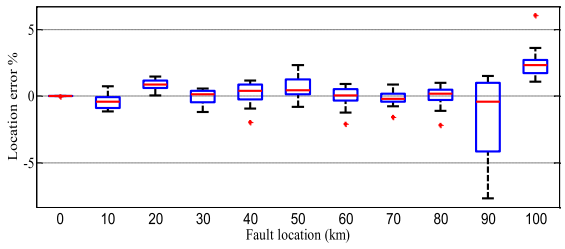

(d) Error between target and output of the trained network

FIGURE 15. Performance and regression analysis of the trained neural network with RTDS results.

synchronous generators (PMSM). The DFIG incorporates partial scale converter units connected between the rotor of the generator and the AC side while the PMSG is integrated via full-scale converters [4].

This part in the paper investigates the impact of AC side grid on the proposed fault location method. For this purpose, a ± 320 kV, 400 km overhead line with MMC units at the terminals is simulated. MMC equivalent components were constructed in PSCAD environment, and the detailed parameters of this system are summarized in [10]. It is worthy to note that the voltage and current signals are sampled at 10 kHz rate and the proposed interpolation strategy presented in section V.A is included during processing. The AC sides for this system include

- 5.2 MVA PMSG unit interfaced by 5 MW 2-level VSC units at one side.
- a conventional AC source at the other side.

As shown in Figs. 16 (a) and 16 (c). The proposed fault location method is implemented in two scenarios:

1- At the terminal at which the conventional AC source is connected as depicted in Fig. 16 (a).
2- At the terminal at which the converter interfaced generation is integrated as depicted in Fig. 16 (c).

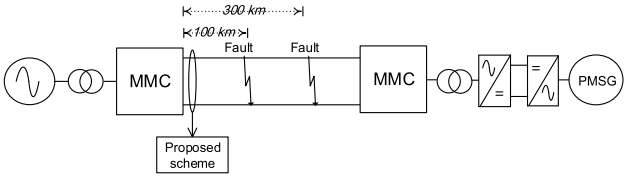

(a) Simulated test system and the proposed location method is implemented according to the 1st scenario.

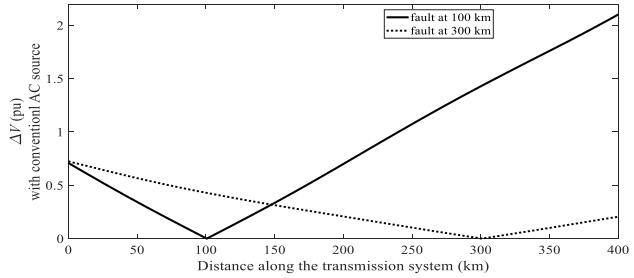

(b) Voltage difference profile with conventional AC source at the AC side.

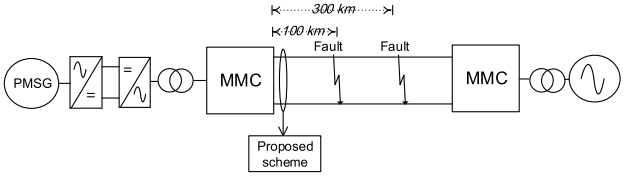

(c) Simulated test system and the proposed method is implemented according to the 2nd scenario.

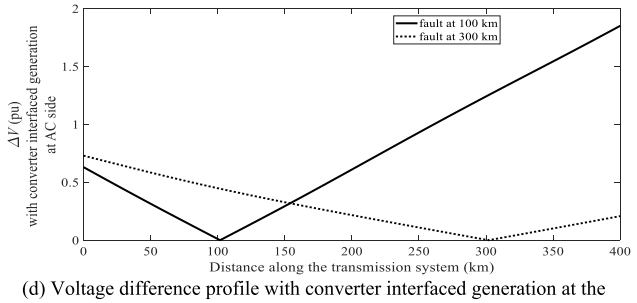

(d) Voltage difference profile with converter interfaced generation at the AC side.

FIGURE 16. Impact of AC side grid on the proposed fault location method.

In both cases, two fault conditions are simulated to validate the proposed fault location method with such systems. Fig. 16 (b) shows the voltage difference profile calculated according to the first scenario. As shown, the minimum value of the derived voltage difference profile successfully indicates the location of the faults at 100 km and 300 km respectively.

For more validation, the proposed method is implemented at the other side according to the second scenario indicated in Fig. 16 (c). The obtained response is almost the same as shown in Fig. 16 (d) where the fault locations are successfully determined in spite of having converter interfaced generation at the AC side.

VII. CONCLUSION

A single-end based fault location method has been proposed for VSC-HVDC transmission systems. There is no need for communication system for the proposed method and hence checking of the synchronization condition between samples is avoided. The proposed method is based on the relationship between the 1-mode and 0-mode voltages of the post-fault condition along the transmission system. The features of the voltage difference profile between the 1-mode and 0-mode help identify the fault location. A neural network has been trained for locating both the pole and ground faults based on a generalized single computation core. The test results have validated the good performance of the proposed method even with uncertain line parameters. The proposed method has been tested with different system configurations, such as bipolar, monopolar, underground cable, and overhead line systems. The tests have been performed based on utilizing collected theoretical samples using PSCAD and that from real time simulation platform RTDS.

APPENDIX

A. BERGERON MODEL EQUATION

The Bergeron model equations for calculating the 1-mode and 0-mode voltages, in terms of single end measurements, at any point along the transmission system are shown in (20) and (21), respectively. The subscripts 1 and 0 are for indicating the 1-mode and 0-mode, respectively. x is the distance at which the voltage components are calculated. v_1, v_0, i_1, i_0 are the locally measured voltage and current signals at one end of the transmission system. Z_c is the characteristic impedance and r is the resistance per unit length. τ is the traveling time along the length x.

$$\begin{aligned} V_{1_{at\ \ x}}(t-\tau_1) &= \frac{1}{2}\left(\frac{Z_{C1}-\frac{r_1x}{4}}{Z_{C1}}\right)^2\left(V_1(t)-i_1(t)\left(Z_{C1}+\frac{r_1x}{4}\right)\right) \\ &+\frac{1}{2}\left(\frac{Z_{C1}-\frac{r_1x}{4}}{Z_{C1}}\right)^2\left(V_1(t-2\tau_1)-i_1(t-2\tau_1)\left(Z_{C1}-\frac{r_1x}{4}\right)\right) \\ &-\left(\frac{\frac{r_1x}{4}}{Z_{C1}}\right)^2 V_1(t-\tau_1)-\frac{r_1x}{4}\left(\frac{Z_{C1}+\frac{r_1x}{4}}{Z_{C1}}\right)\left(\frac{Z_{C1}-\frac{r_1x}{4}}{Z_{C1}}\right) \\ &\times i_1(t-\tau_1) \end{aligned} \tag{20}$$

$$\begin{aligned} V_{0_{at\ \ x}}(t-\tau_0) &= \frac{1}{2}\left(\frac{Z_{C0}-\frac{r_0x}{4}}{Z_{C0}}\right)^2\left(V_0(t)-i_0(t)\left(Z_{C0}+\frac{r_0x}{4}\right)\right) \\ &+\frac{1}{2}\left(\frac{Z_{C0}-\frac{r_0x}{4}}{Z_{C0}}\right)^2\left(V_0(t-2\tau 0)-i_0(t-2\tau 0)\left(Z_{C0}-\frac{r_0x}{4}\right)\right) \\ &-\left(\frac{\frac{r_0x}{4}}{Z_{C0}}\right)^2 V_0(t-\tau_0)-\frac{r_0x}{4}\left(\frac{Z_{C0}+\frac{r_0x}{4}}{Z_{C0}}\right)\left(\frac{Z_{C0}-\frac{r_0x}{4}}{Z_{C0}}\right) i_0 \\ &\times(t-\tau_0) \end{aligned} \tag{21}$$

B. BIPOLAR AND MONOPOLAR SYSTEMS CONFIGURATIONS

The bipolar and monopolar systems are different in configuration. In bipolar system, each terminal has two converter units while the monopolar system has only single converter unit at each end [38], [39]. Fig. 17 shows the configuration

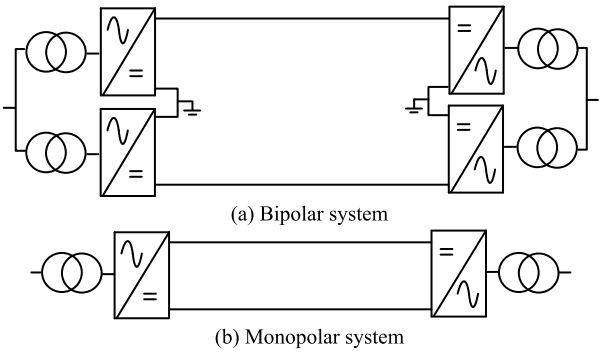

FIGURE 17. Bipolar and monopolar systems configurations [38], [39].

of both systems. The bipolar system is considered as two monopolar systems combined together [38], [39].

The proposed theory works for both types. There is no problem when applying the proposed theory with monopolar and bipolar systems. In both cases, the 1-mode and 0-mode voltage components could be calculated in terms of the local measured signals. All the proposed analysis and equations are applicable with both types.

The difference between the monopolar and bipolar systems is highlighted in case of ground fault condition as discussed in the following paragraph. However, this difference does not affect the proposed fault location method.

In case of pole-to-ground fault, the DC line voltage, in bipolar systems, is reduced to half of its nominal level. The ground fault in bipolar system is considered as a short circuit on one of the two converters at DC terminals. On the other side, with the monopolar system, the DC link voltage is not reduced with ground fault condition. However, the faulted pole become grounded at zero voltage while the other pole voltage is raised to the total system voltage value. This is indicated in the Table 6 for more elaboration.

The proposed method works well with both bipolar and monopolar systems because it is manly depending on the voltage profile along the transmission system which is highly affected in both systems. This is a good advantage of the proposed method as it is a general method and the included results in the manuscript provide evidence about the high efficacy of the proposed method for the bipolar and monopolar systems.

TABLE 6. Difference between bipolar and monopolar system considering ground fault condition.

Bipolar system		Monopolar system	
Before the fault	After the fault*	Before the fault	After the fault*
$\|Vp\|$= 0.5 pu	$\|Vp\|$= 0.0 pu	$\|Vp\|$= 0.5 pu	$\|Vp\|$= 0.0 pu
$\|Vn\|$= 0.5 pu	$\|Vn\|$= 0.5 pu	$\|Vn\|$= 0.5 pu	$\|Vn\|$= 1.0 pu

* Assuming that the fault is on the positive pole

ACKNOWLEDGMENT

The authors would like to thank Prof. Tamer Kawady and Prof. Nagy Elkalashy from Menoufia University, Egypt, for the provided discussions and help. They also like to thank Dr. Jianing Li from Birmingham University, U.K., for the technical support provided to work on RTDS.

REFERENCES

[1] N. Flourentzou, V. G. Agelidis, and G. D. Demetriades, "VSC-based HVDC power transmission systems: An overview," *IEEE Trans. Power Electron.*, vol. 24, no. 3, pp. 592–602, Mar. 2009.
[2] Y. Fu, C. Wang, W. Tian, and M. Shahidehpour, "Integration of large-scale offshore wind energy via VSC-HVDC in day-ahead scheduling," *IEEE Trans. Sustain. Energy*, vol. 7, no. 2, pp. 535–545, Apr. 2016.
[3] A. Xue, J. Zhang, L. Zhang, Y. Sun, J. Cui, and J. Wang, "Transient frequency stability emergency control for the power system interconnected with offshore wind power through VSC-HVDC," *IEEE Access*, vol. 8, pp. 53133–53140, 2020.
[4] M. I. Hossain and M. A. Abido, "Positive-negative sequence current controller for LVRT improvement of wind farms integrated MMC-HVDC network," *IEEE Access*, vol. 8, pp. 193314–193339, 2020.
[5] R. L. Sellick and M. Åkerberg, "Comparison of HVDC light (VSC) and HVDC classic (LCC) site aspects, for a 500 MW 400 kV HVDC transmission scheme," in *Proc. 10th IET Int. Conf. AC DC Power Transmiss. (ACDC)*, Birmingham, U.K., 2012, pp. 1–6.
[6] Y. Xue, X.-P. Zhang, and C. Yang, "Elimination of commutation failures of LCC HVDC system with controllable capacitors," *IEEE Trans. Power Syst.*, vol. 31, no. 4, pp. 3289–3299, Jul. 2016.
[7] G. Li, J. Liang, T. Joseph, T. An, J. Lu, M. Szechtman, B. R. Andersen, and Q. Zhuang, "Feasibility and reliability analysis of LCC DC grids and LCC/VSC hybrid DC grids," *IEEE Access*, vol. 7, pp. 22445–22456, 2019.
[8] X.-P. Zhang, "Multiterminal voltage-sourced converter-based HVDC models for power flow analysis," *IEEE Trans. Power Syst.*, vol. 19, no. 4, pp. 1877–1884, Nov. 2004.
[9] M. Elgeziry, M. Elsadd, N. Elklashy, T. Kawady, A. Taalab, and M. Izzularab, "Non-pilot protection method for multiterminal VSC-HVDC transmission systems," *IET Renew. Power Gener.*, vol. 13, no. 16, pp. 3033–3042, Dec. 2019.
[10] M. M. Elgamasy, A.-M.-I. Taalab, T. A. Kawady, M. A. Izzularab, and N. I. Elkalashy, "Wave propagation differential protection scheme for VSC-HVDC transmission systems," *Electr. Power Syst. Res.*, vol. 189, Dec. 2020, Art. no. 106826.
[11] M. M. Elgamasy, A.-M. I. Taalab, T. A. Kawady, M. A. Izzularab, and N. I. Elkalashy, "Virtual difference voltage scheme for fault detection in VSC-HVDC transmission systems," *J. Modern Power Syst. Clean Energy*, vol. 8, no. 5, pp. 991–1004, 2020.
[12] R. Ara, U. A. Khan, A. I. Bhatti, and B. W. Lee, "A reliable protection scheme for fast DC fault clearance in a VSC-based meshed MTDC grid," *IEEE Access*, vol. 8, pp. 88188–88199, 2020.
[13] X. Pei, H. Pang, Y. Li, L. Chen, X. Ding, and G. Tang, "A novel ultra-high-speed traveling-wave protection principle for VSC-based DC grids," *IEEE Access*, vol. 7, pp. 119765–119773, 2019.
[14] Q. Huai, K. Liu, L. Qin, X. Liao, S. Zhu, Y. Li, and H. Ding, "Backup-protection scheme for multi-terminal HVDC system based on wavelet-packet-energy entropy," *IEEE Access*, vol. 7, pp. 49790–49803, 2019.
[15] J. A. Ansari, C. Liu, and S. A. Khan, "MMC based MTDC grids: A detailed review on issues and challenges for operation, control and protection schemes," *IEEE Access*, vol. 8, pp. 168154–168165, 2020.
[16] Y. Wang, Z. Hao, B. Zhang, and F. Kong, "A pilot protection scheme for transmission lines in VSC-HVDC grid based on similarity measure of traveling waves," *IEEE Access*, vol. 7, pp. 7147–7158, 2019.
[17] J. Suonan, S. Gao, G. Song, Z. Jiao, and X. Kang, "A novel fault-location method for HVDC transmission lines," *IEEE Trans. Power Del.*, vol. 25, no. 2, pp. 1203–1209, Apr. 2010.
[18] L. Yuansheng, W. Gang, and L. Haifeng, "Time-domain fault-location method on HVDC transmission lines under unsynchronized two-end measurement and uncertain line parameters," *IEEE Trans. Power Del.*, vol. 30, no. 3, pp. 1031–1038, Jun. 2015.
[19] J.-Y. Wu, S. Lan, S.-J. Xiao, and Y.-B. Yuan, "Single pole-to-ground fault location system for MMC-HVDC transmission lines based on active pulse and CEEMDAN," *IEEE Access*, vol. 9, pp. 42226–42235, 2021.

[20] C. Xing, S. Li, and X. Xi, "Research on a fault location method for a pole-to-pole short-circuit fault in an LCC-MMC hybrid DC transmission system," *IEEE Access*, vol. 8, pp. 165683–165692, 2020.
[21] R. Rohani and A. Koochaki, "A hybrid method based on optimized neuro-fuzzy system and effective features for fault location in VSC-HVDC systems," *IEEE Access*, vol. 8, pp. 70861–70869, 2020.
[22] O. M. K. K. Nanayakkara, A. D. Rajapakse, and R. Wachal, "Traveling-wave-based line fault location in star-connected multiterminal HVDC systems," *IEEE Trans. Power Del.*, vol. 27, no. 4, pp. 2286–2294, Oct. 2012.
[23] O. M. K. K. Nanayakkara, A. D. Rajapakse, and R. Wachal, "Location of DC line faults in conventional HVDC systems with segments of cables and overhead lines using terminal measurements," *IEEE Trans. Power Deliv.*, vol. 27, no. 1, pp. 279–288, Jan. 2012.
[24] P. Chen, B. Xu, and J. Li, "A traveling wave based fault locating system for HVDC transmission lines," in *Proc. Int. Conf. Power Syst. Technol.*, Chongqing, China, Oct. 2006, pp. 1–4.
[25] Q. Huai, L. Qin, K. Liu, H. Ding, X. Liao, and T. Tan, "Combined line fault location method for MMC–HVDC transmission systems," *IEEE Access*, vol. 8, pp. 170794–170806, 2020.
[26] Y. Ma, H. Li, G. Wang, and J. Wu, "Fault analysis and traveling-wave-based protection scheme for double-circuit LCC-HVDC transmission lines with shared towers," *IEEE Trans. Power Del.*, vol. 33, no. 3, pp. 1479–1488, Jun. 2018.
[27] C. Zhang, G. Song, T. Wang, L. Wu, and L. Yang, "Non-unit traveling wave protection of HVDC grids using Levenberg-Marquart optimal approximation," *IEEE Trans. Power Del.*, vol. 35, no. 5, pp. 2260–2271, Oct. 2020.
[28] C. Zhang, G. Song, T. Wang, and L. Yang, "Single-ended traveling wave fault location method in DC transmission line based on wave front information," *IEEE Trans. Power Del.*, vol. 34, no. 5, pp. 2028–2038, Oct. 2019.
[29] T. Bi, S. Wang, and K. Jia, "Single pole-to-ground fault location method for MMC-HVDC system using active pulse," *IET Gener., Transmiss. Distrib.*, vol. 12, no. 2, pp. 272–278, Jan. 2018.
[30] G. Song, T. Wang, and K. S. T. Hussain, "DC line fault identification based on pulse injection from hybrid HVDC breaker," *IEEE Trans. Power Del.*, vol. 34, no. 1, pp. 271–280, Feb. 2019.
[31] G.-Y. Kwon, C.-K. Lee, G. Seok Lee, Y. Ho Lee, S. Jin Chang, C.-K. Jung, J.-W. Kang, and Y.-J. Shin, "Offline fault localization technique on HVDC submarine cable via time–frequency domain reflectometry," *IEEE Trans. Power Del.*, vol. 32, no. 3, pp. 1626–1635, Jun. 2017.
[32] M. Bawart, M. Marzinotto, and G. Mazzanti, "Diagnosis and location of faults in submarine power cables," *IEEE Elect. Insul. Mag.*, vol. 32, no. 4, pp. 24–37, Jul. 2016.
[33] M. Farshad and J. Sadeh, "A novel fault-location method for HVDC transmission lines based on similarity measure of voltage signals," *IEEE Trans. Power Del.*, vol. 28, no. 4, pp. 2483–2490, Oct. 2013.
[34] D. Tzelepis, S. Mirsaeidi, A. Dysko, Q. Hong, J. He, and C. D. Booth, "Intelligent fault location in MTDC networks by recognizing patterns in hybrid circuit breaker currents during fault clearance process," *IEEE Trans. Ind. Informat.*, vol. 17, no. 5, pp. 3056–3068, May 2021, doi: 10.1109/TII.2020.3003476.
[35] G. Luo, C. Yao, Y. Liu, Y. Tan, J. He, and K. Wang, "Stacked auto-encoder based fault location in VSC-HVDC," *IEEE Access*, vol. 6, pp. 33216–33224, 2018.
[36] G. Song, X. Chu, X. Cai, S. Gao, and M. Ran, "A fault-location method for VSC-HVDC transmission lines based on natural frequency of current," *Int. J. Elect. Power Energy Syst.*, vol. 63, pp. 347–352, Dec. 2014.
[37] J. Xu, Y. Lu, C. Zhao, and J. Liang, "A model-based DC fault location scheme for multi-terminal MMC-HVDC systems using a simplified transmission line representation," *IEEE Trans. Power Del.*, vol. 35, no. 1, pp. 386–395, Feb. 2020.
[38] N. R. Watson and J. D. Watson, "An overview of HVDC technology," *Energies*, vol. 13, no. 17, p. 4342, Aug. 2020.
[39] G. Tang, Z. He, and H. Pang, "R&D and application of voltage sourced converter based high voltage direct current engineering technology in China," *J. Modern Power Syst. Clean Energy*, vol. 2, no. 1, pp. 1–15, Jan. 2014.

MAHMOUD M. ELGAMASY received the B.Sc., M.Sc., and Ph.D. degrees from Menoufia University, Egypt, in 2011, 2015, and 2021, respectively. He was a Postgraduate Research Visiting Student with Birmingham University, Birmingham, U.K., under joint supervision program with Menoufia University for pursuing the Ph.D. degree in electrical engineering. From January 2012 to February 2015, he was a Teaching Assistant and from February 2015 to February 2021, he was an Assistant Lecturer. He is currently a Lecturer with the Electrical Power and Machines Engineering Department, Menoufia University. His research interests include power systems protection, renewable wind energy resources, and high voltage direct current transmission systems.

MOHAMED A. IZZULARAB received the B.Sc. degree in electrical engineering from Menoufia University, Egypt, in 1973, the M.Sc. degree from El-Mansoura University, in 1978, the Dr.Ing. degree from I.N.P.T. Toulouse, France, in 1983, and the D.Sc. degree in electrical engineering from Paul Sabatier University Toulouse, France, in 1987. He joined the Department of Electrical Engineering, Menoufia University, as a Lecturer, in 1983, where he was promoted as an Associate Professor, in 1988. Since 1992, he has been working as a Full Professor with the Department of Electrical Engineering, Faculty of Engineering, Menoufia University. He is also leading the Research Group of High Voltage Engineering and Dielectric Materials. He was appointed as the Vice-President of Menoufia University for community service and environmental development, from 2006 to 2007, and the President of Menoufia University, from 2007 to 2011.

XIAO-PING ZHANG (Fellow, IEEE) is currently a Professor of electrical power systems with the University of Birmingham, U.K. He is also the Director of smart grid with the Birmingham Energy Institute and the Co-Director of the Birmingham Energy Storage Center. He coauthored the first and second edition of the monograph *Flexible AC Transmission Systems: Modeling and Control* (Springer, in 2006 and 2012). He coauthored the book *Restructured Electric Power Systems: Analysis of Electricity Markets with Equilibrium Models* (IEEE Press/Wiley, in 2010). His research interests include modeling and control of HVDC, FACTS and wind/wave generation, distributed energy systems and market operations, and power system planning. He has been made a fellow of IEEE "for contributions to modeling and control of high-voltage DC and AC transmission systems." He is also a fellow of IET. He is an IEEE PES Distinguished Lecturer on HVDC, FACTS, and wave energy generation. He has been an Advisor to IEEE PES U.K. and Ireland Chapter and chairing the IEEE PES WG on Test Systems for Economic Analysis. He has been appointed to the Expert Advisory Group, U.K. Government's Offshore Transmission Network Review, since 2020.